

UC San Diego

UC San Diego Previously Published Works

Title

Glycocalyx crowding with mucin mimetics strengthens binding of soluble and virus-associated lectins to host cell glycan receptors

Permalink

<https://escholarship.org/uc/item/341956rm>

Journal

Proceedings of the National Academy of Sciences of the United States of America, 118(40)

ISSN

0027-8424

Authors

Honigfort, Daniel J
Altman, Meghan O
Gagneux, Pascal
et al.

Publication Date

2021-10-05


DOI

10.1073/pnas.2107896118

Peer reviewed



Glycocalyx crowding with mucin mimetics strengthens binding of soluble and virus-associated lectins to host cell glycan receptors

Daniel J. Honigfort^{a,1}, Meghan O. Altman^{b,2}, Pascal Gagneux^b , and Kamil Godula^{a,3}

^aDepartment of Chemistry and Biochemistry, University of California San Diego, La Jolla, CA 92093-0358; and ^bDepartment of Pathology, University of California San Diego, La Jolla, CA 92093-0687

Edited by Barbara Imperiali, Massachusetts Institute of Technology, Cambridge, MA, and approved August 19, 2021 (received for review May 10, 2021)

Membrane-associated mucins protect epithelial cell surfaces against pathogenic threats by serving as nonproductive decoys that capture infectious agents and clear them from the cell surface and by erecting a physical barrier that restricts their access to target receptors on host cells. However, the mechanisms through which mucins function are still poorly defined because of a limited repertoire of tools available for tailoring their structure and composition in living cells with molecular precision. Using synthetic glycopolymer mimetics of mucins, we modeled the mucosal glycocalyx on red blood cells (RBCs) and evaluated its influence on lectin (SNA) and virus (H1N1) adhesion to endogenous sialic acid receptors. The glycocalyx inhibited the rate of SNA and H1N1 adhesion in a size- and density-dependent manner, consistent with the current view of mucins as providing a protective shield against pathogens. Counterintuitively, increasing the density of the mucin mimetics enhanced the retention of bound lectins and viruses. Careful characterization of SNA behavior at the RBC surface using a range of biophysical and imaging techniques revealed lectin-induced crowding and reorganization of the glycocalyx with concomitant enhancement in lectin clustering, presumably through the formation of a more extensive glycan receptor patch at the cell membrane. Our findings indicate that glycan-targeting pathogens may exploit the biophysical and biomechanical properties of mucins to overcome the mucosal glycocalyx barrier.

influenza A | lectins | glycocalyx | mucin | biophysics

Many viral and bacterial pathogens that circulate in the human population, and continuously pose a risk of disease outbreaks and pandemics, utilize glycans on host cells to facilitate their adhesion and initiate infection (1). Sialic acids (Sias) represent one example of a cell surface glycan receptor frequently targeted by pathogens, such as the influenza A virus (IAV) among others (Fig. 1A). Sias are monosaccharides typically added as a terminal modification to more complex glycans of membrane-associated glycoproteins or glycolipids and, as a result, are prominently displayed at high concentrations on mammalian cells (2). There, they are involved in a spectrum of cellular processes, such as adhesion, migration, or communication (3), and help regulate vital organismal functions, including fertilization, development, and immunity (4). The regiochemical configuration of the glycosidic bond that links Sias to the underlying glycan, typically a galactose residue, defines the host specificity of IAVs. Although specific sialoglycan receptor structures required for IAV infection are yet to be defined, α 2,3-linked and α 2,6-linked Sias are generally considered to be determinants for avian and human viruses, respectively (5). Modification of Sias through *O*-acetylation (6) or *N*-glycolylation (7) further increases the structural diversity and functional range of IAV receptors, and sulfation (8) and phosphorylation (9) of asialoglycans alone may be sufficient for viral binding and infection (10). Pathogen-associated proteins that recognize Sias, such as hemagglutinins (HA) in the case of IAVs, often share a low-affinity binding site for the individual receptor structures but achieve high-avidity binding to Sias displayed on cells through oligomerization and multivalency (2, 11, 12).

In response to the constant pathogenic challenge, the cells of mucosal epithelial tissues, which are most susceptible to infection, express soluble and membrane-bound glycoproteins called mucins to limit pathogen adhesion and spread (Fig. 1A) (13, 14). Comprising long polypeptide chains densely decorated with glycans (Fig. 1B), membrane-associated mucins provide a dual protective function against infection by forming a dense extended biopolymer brush, restricting access to the cell surface, and by presenting decoy receptors to capture and clear the pathogen (13, 15). Both the biophysical barrier (16) and the receptor decoy (17) functions of mucins have been shown to limit bacterial and viral infection, including by IAVs. The interactions between pathogens and mucins based on glycan recognition have received substantial attention, enabled by the emergence of powerful glycomics screening platforms integrating either chemically or chemoenzymatically produced *O*-glycopeptides (18) or naturally (19) and genetically (20) derived mucin structures. By contrast, the biophysical mechanisms allowing mucins to limit infection are yet to be examined experimentally in a systematic way. This is primarily due to the lack of tools for manipulating the architecture and glycosylation status of mucins with molecular precision in living cells (21). Membrane engineering with synthetic glycopolymers (GPs), which mimic the architecture and properties of mucins and can be chemically defined at the molecular level (22, 23), has emerged as a convenient approach to study phenomena associated with the mucin glycocalyx,

Significance

Like other animal hosts, humans are constantly challenged by pathogens. This has led to an evolution of physical barriers coating all mucosal tissues, which are most vulnerable to infection. An important part of this defense is a dense brush of large proteins, called mucins, which are heavily decorated with sugars and keep pathogens at bay. Deciphering how pathogens overcome the mucin barrier is necessary to understand early stages of infection and to develop more effective treatments. By artificially installing a mucin-like shield on the surfaces of cells using synthetic sugar-bearing polymers, we have discovered a physical mechanism by which proteins and viruses can exploit this barrier to adhere to their targets more strongly.

Author contributions: D.J.H., P.G., and K.G. designed research; D.J.H. and M.O.A. performed research; M.O.A. contributed new reagents/analytic tools; D.J.H., M.O.A., and K.G. analyzed data; and D.J.H., P.G., and K.G. wrote the paper.

The authors declare no competing interest.

This article is a PNAS Direct Submission.

Published under the PNAS license.

¹Present address: R&D Department, Element Biosciences, San Diego, CA 92121.

²Present address: R&D Department, Abbott Labs, Carlsbad, CA 92008.

³To whom correspondence may be addressed. Email: kgodula@ucsd.edu.

This article contains supporting information online at <https://www.pnas.org/lookup/suppl/doi:10.1073/pnas.2107896118/-DCSupplemental>.

Published September 28, 2021.

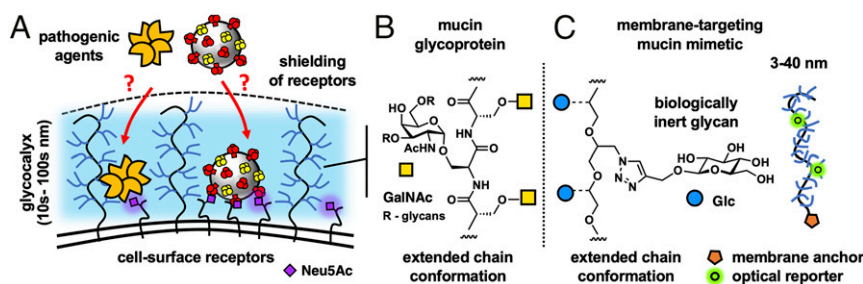


Fig. 1. The mucosal glycoalkyl provides a physical barrier against pathogen association with host cells. (A) A brush of membrane-associated mucin glycoproteins restricts the ingress of pathogens toward cell surface glycan receptors, such as Sias. (B) The extended conformation of mucins and their physical properties arise from dense glycosylation of their core peptide backbone. (C) Cell surface targeting GPs based on a linear PEO scaffold, which mimic the architecture and physical properties of mucins, are used to investigate mechanisms through which pathogens can breach the protective mucosal glycoalkyl barrier.

including its interactions with sialic acid-binding proteins (24) and the effects of its biophysical properties on cellular interactions and functions (25, 26). We have recently observed that introducing mucin mimetics to the surfaces of cells resulted in increased glycoalkyl crowding, which limited lectin binding to membrane-associated glycoconjugates (27). Bertozzi and coworkers (28) further showed that mucin mimetics based on synthetic glycopeptides imbedded in supported lipid bilayers (SLBs) could shield sialylated glycosphingolipids from H1N1. Studies with synthetic mucin analogs can, thus, reveal mechanistic insights into how mucins may limit pathogen adhesion through biophysical means.

To counteract the protective mucin shield, many pathogens express enzymes that degrade mucins (29, 30) or change their glycosylation status (31). While the complete removal of mucins by microbial proteases disrupts the integrity of the glycoalkyl and exposes the cell surface to pathogen attack, the removal of only their receptor decoys with glycosidases, such as the IAV neuraminidase (NA), leaves the physical mucin barrier intact. The mechanism through which pathogens that do not break down the mucin shield overcome this physical barrier are yet to be fully investigated.

In this study, we have deployed synthetic GPs with tunable lengths (Fig. 1C) to model membrane-associated mucin displays on the surfaces of avian (turkey) red blood cells (RBCs) and examined how the mucin mimetic glycoalkyl size and density influenced the kinetics and thermodynamics of lectin (SNA) and viral (H1N1) binding to endogenous glycan receptors. By employing mucin mimetics bearing glucose residues, which are refractory to SNA and H1N1 binding, we were able to identify changes in SNA and H1N1 association stemming from altered physical properties of the glycoalkyl. We have observed polymer length-dependent inhibition of SNA and H1N1 adhesion to their cell surface receptors in the presence of the membrane-tethered mucin mimetic brush, providing further support for the mucin shield model. We have also identified a biophysical mechanism by which lectins and viruses exploit the crowded glycoalkyl to strengthen their association with the cell.

Results

Glycoalkyl Engineering with Mucin Mimetics Alters RBC Morphology and Properties. To model key physical features of the epithelial glycoalkyl, that is, its dense, extended brush-like organization of mucin glycoproteins, we have generated synthetic mucin mimetic GPs with defined length and glycosylation (Fig. 1C). The mucin mimetic GPs (Fig. 2A) were assembled on linear hydrophilic poly(ethylene oxide) (PEO) scaffolds of increasing length (degree of polymerization [DP] = 30, 140, 440) and with narrow dispersity ($\mathcal{D} < 1.3$). The precursor backbones were generated via controlled anionic ring-opening polymerization of epichlorohydrin (32) followed by functionalization with azide side chains for the attachment of propargyl glycosides via copper-catalyzed azide alkyne

cycloaddition (CuAAC) (33) (*SI Appendix, Scheme S1*). The efficiency of this “click” process resulted in a high frequency of glycosylated side chains in close proximity to the PEO backbone, forcing the GPs into extended conformations characteristic of mucins (27, 34). Seeking to isolate the biophysical properties of mucins from their glycan interactions, we modified our GPs with glucose, a monosaccharide typically not found in mucin glycans (Fig. 1). This produced mucin mimetic “spectators” lacking Sia receptors for IAVs but able to tune the size and density of the glycoalkyl. The mucin mimetics were also endowed with a hydrophobic 4,5-*seco*-cholesten-5-one end-group for anchoring of the GPs in cell membranes, and a small fraction (<1%) of their side chains were labeled with AlexaFluor 488 (AF488) or cyanine 3 (Cy3) dyes for detection via fluorescence (Fig. 1). To examine the impact of glycoalkyl size on molecular recognition events at the cell surface, we generated short (GP-S, DP = 30), medium (GP-M, DP = 140), and long (GP-L, DP = 440) mucin mimetics (Fig. 2A and B) (27).

RBCs provide a useful model for examining the effects of glycoalkyl properties on lectin and IAV interactions with sialoglycan receptors. RBCs present endogenous Sia modifications in both α 2,3 and α 2,6 linkages and are commonly used to assess IAV binding activity via cell hemagglutination. Even though this cell type is not the target of IAV infection in mammals, RBCs offer a platform to study mucin-related phenomena by providing an intermediary between simple laboratory membrane models based on SLBs or lipid vesicles with chemically defined glycoconjugates and the dynamic and heterogeneous environment of the epithelial cell glycoalkyl. The RBCs present a compositionally complex but compact native glycoalkyl (~5 nm to 10 nm) (35), which can be augmented with GPs to introduce extended mucin-like features. At the same time, RBCs lack endocytic activity, which allows for installing mucin mimetic brushes at high density and compositional stability.

To introduce mucin-like features into the RBC glycoalkyl, the cells were treated with the lipid-terminated GPs of all three lengths at increasing concentrations ($c_{GP} = 0.05 \mu\text{M}$ to $50.00 \mu\text{M}$) for 1 h. Membrane incorporation of the fluorescently labeled polymers was measured by flow cytometry (Fig. 2C). The efficiency of membrane insertion was inversely proportional to polymer length, resulting in increasingly extended but less dense glycoalkyl structures when the cells were treated at equal polymer concentrations. Polymers lacking the *seco*-cholestenone hydrophobic anchor did not insert into the cell membranes (*SI Appendix, Fig. S8*).

Examination of the cells with light microscopy revealed pronounced rounding and loss of membrane features with increasing incorporation of the medium and long polymers (Fig. 2D; shown for GP-L). Flow cytometry analysis of RBCs after treatment with mucin mimetics of all three lengths ($c_{GP} = 50 \mu\text{M}$) showed negative correlation between GP length and side scatter with little

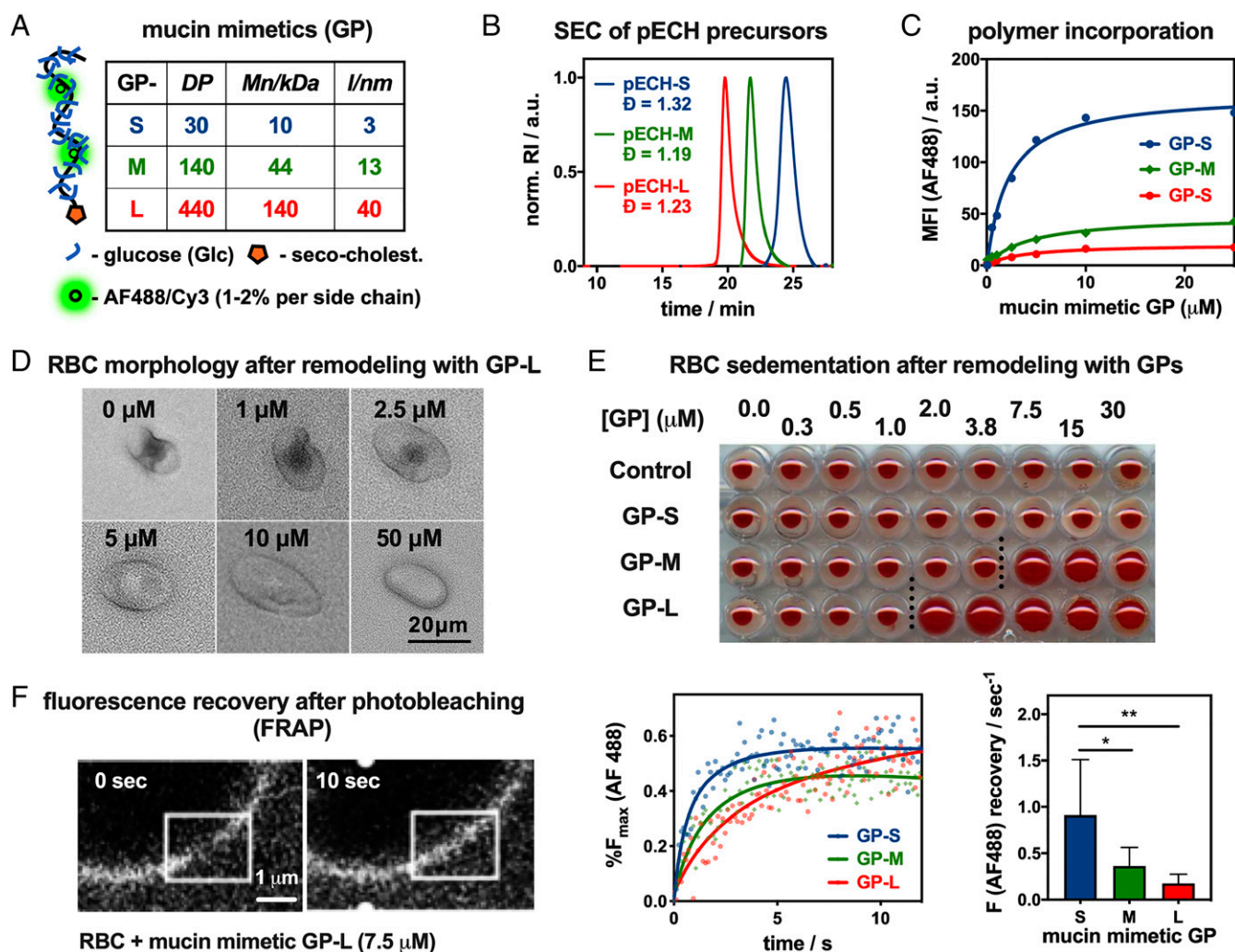


Fig. 2. Construction and characterization of a mucosal glycolyx model. (A) Short (S), medium (M), and long (L) mucin mimetic GPs ranging in size from ~ 3 nm to 40 nm were generated from poly(epichlorohydrin) (pECH) precursors (M_n , number average molecular weight; l , estimated end to end length). (B) Size-exclusion chromatography (SEC) of pECH precursors indicates narrow molecular weight distributions of the polymer scaffolds. The polymers were modified with biologically inert glucose side chains, fluorescent probes (AF488 or Cy3) for visualization, and chain end-terminated with hydrophobic cholesterol membrane anchor. RI = refractive index. (C) Incorporation of AF488-labeled mucin mimetics GPs into RBC membranes was analyzed by flow cytometry. MFI = median fluorescence intensity. (D) Optical microscopy and light scattering reveal increased cell rounding with increasing glycolyx density (shown for GP-L). (E) Sedimentation of RBCs remodeled with increasing concentration of all three GPs ($c_{GP} = 0.25 \mu\text{M}$ to $30 \mu\text{M}$). (F) FRAP analysis shows length-dependent diffusion of AF488-labeled mucin mimetics GP in RBC membranes. White overlaid boxes draw attention to the photobleached region. Lines represent the average signal from $n = 6$ cells, $c_{GP} = 7.5 \mu\text{M}$; P values were determined by one-way ANOVA with multiple comparisons ($* < 0.05$, $** < 0.01$).

change in forward scatter intensity (SI Appendix, Fig. S9). This supports the visual observation of a polymer size-dependent decrease in cell complexity without significant alterations of the overall cell size (Fig. 2D). The changes in cell morphology likely arise from entropic pressures exerted on the cell membrane upon a mushroom-to-brush conformational transition of the tethered mucin mimetics in response to glycolyx crowding, as proposed recently by Paszek and coworkers (36) in their analysis of the role of mucins in cell shape regulation. The transition in cell shape was accompanied by changes in sedimentation properties of the remodeled RBCs. We identified polymer concentration thresholds of ~ 7.5 and $2.0 \mu\text{M}$ for GP-M and GP-L, respectively, above which cell sedimentation becomes less efficient (Fig. 2E). No such effect was detected for the shortest polymers GP-S over the tested range of concentrations. RBC aggregation and sedimentation are processes facilitated by the cells' discoid shape and surface charge, which are both features affected by the introduction of the extended mucin-like glycolyx (37).

The morphological changes in the cells induced by the mucin mimetics indicate an increase in glycolyx crowding, which should likewise influence the lateral membrane diffusion of the GPs. Taking advantage of the fluorophore labels present in the polymers, we performed fluorescence recovery after photobleaching (FRAP) analysis on cells treated with GPs of all three lengths at the threshold concentration, $c_{GP} = 7.5 \mu\text{M}$, at which the medium-size mucin mimetic GP-M induced alterations in cell shape and sedimentation properties (Fig. 2F). This concentration is above the transition concentration for the long polymer GP-L and close to the surface saturation level for the short mimetic, GP-S, which did not alter sedimentation. The FRAP analysis revealed that all three GPs showed lateral diffusion within the endogenous glycolyx, with fluorescence recovery rates decreasing from $0.91 \pm 0.24 \text{ s}^{-1}$ for GP-S, to $0.36 \pm 0.08 \text{ s}^{-1}$ for GP-M, to $0.18 \pm 0.04 \text{ s}^{-1}$ for the longest polymer, GP-L. Considering that the cell surface grafting efficiency for GP-S is significantly higher than for GP-M and GP-L (SI Appendix, Fig. S7), the mobility of the mucin mimetics

in the glycocalyx is, thus, influenced more strongly by their size rather than their density in the membrane.

Mucin Mimetics Slow the Rate of Lectin Association while Enhancing Binding Complex Stability. We examined the effects of the mucin mimetic glycocalyx size and density on the binding of *Sambucus nigra* agglutinin (SNA) to Sias on RBCs. Cells treated with GPs of all three lengths near the threshold concentration for inducing cell morphology change ($c_{GP} = 7.5 \mu M$) were incubated with a fluorescently labeled (AF647) SNA lectin at subagglutination concentration ($c_{SNA} = 0.2 \mu g/mL$). The lectin binding was assessed via flow cytometry at regular time points until signal saturation (~ 13 min), and the resulting data were fitted and benchmarked to untreated control cells to determine the relative rates (r_{rel}) of binding for each condition (Fig. 3A). GP-M and GP-L reduced the rates of SNA binding to a similar extent ($r_{rel} = 0.84 \pm 0.05$ and $0.88 \pm 0.05 s^{-1}$, respectively), while the shortest mucin mimetic, GP-S, had no effect on the extent or rate of lectin association ($r_{rel} = 1.02 \pm 0.05$). These observations are consistent with GP shielding of endogenous glycan receptors (28) according to their size and is expected based on the dimensions of the RBC glycocalyx (~ 10 nm) and the lengths of the different mucin mimetics ($\sim 3, 13,$ and 40 nm; Fig. 2A).

To assess the effects of the mucin mimetics on lectin retention at the cell surface, the remodeled RBCs were allowed to reach saturation binding with SNA (15 min), washed, and allowed to reequilibrate in fresh phosphate-buffered saline (30 min). Flow cytometry was used to monitor the retention of the fluorescent SNA by RBCs over the course of the experiment, and the percentage of SNA remaining at equilibrium was calculated (Fig. 3B). Polymers of all three lengths enhanced SNA retention by ~ 8 to

11% over untreated control cells. In contrast to lectin association, the impact of polymer length on SNA retention was much less pronounced, with the shortest polymer GP-S also exerting significant effect. This points to a change in the avidity of the SNA-receptor binding complex driven by polymer density rather than size. Fluorescence confocal microscopy showed increased exclusion of the mucin mimetics from SNA (Fig. 3C; $c_{GP} = 7.5 \mu M$, $c_{SNA} = 0.2 \mu g/mL$), suggesting extensive lectin clustering in the presence of the polymers. Pearson's correlation analysis (R^2 values) showed a decrease in GP colocalization with SNA according to size (GP-S, $R^2 = 0.53 \pm 0.17$; GP-M, $R^2 = 0.38 \pm 0.17$; GP-L, $R^2 = 0.27 \pm 0.16$).

Our experiments indicate that increasing mucin mimetic size inhibits lectin association, and membrane crowding promotes the formation of more stable adhesion complexes, presumably through lectin clustering. In the mucin glycocalyx, which can be described as a surface-tethered polymer brush (36), the extension of the glycoproteins away from the membrane can be driven by crowding. Similar behavior was also recently confirmed for synthetic GPs in SLBs (28). To evaluate the effect of mucin mimetic density in the RBC glycocalyx on SNA interactions, we determined equilibrium binding and retention of SNA at increasing membrane densities for the medium-sized polymer GP-M ($c_{GP,M} = 0.1 \mu M$ to $50.0 \mu M$). We observed an emergence of SNA shielding at a polymer concentration of $6.4 \mu M$ (Fig. 3D), which also coincided with the transition of the RBCs toward a more rounded phenotype with altered sedimentation properties (Fig. 2E). Likewise, SNA dissociation became significantly inhibited at this threshold concentration (Fig. 3D). Together, these observations support a density-dependent transition of the GPs from coiled to extended conformations in the

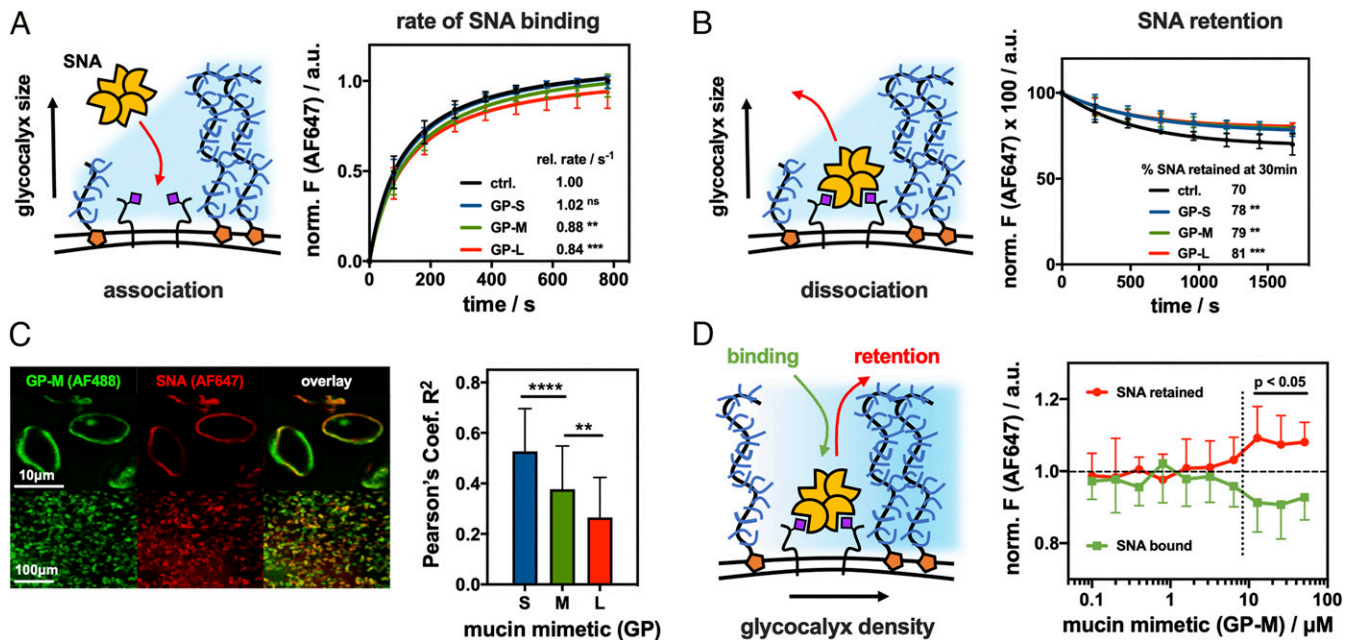


Fig. 3. Spectator glycocalyx size and density regulate SNA interactions with cell surface receptors. (A) Extended glycocalyx reduces the rate of SNA binding. RBCs were remodeled with S, M, and L mucin mimetics GP ($c_{GP} = 7.5 \mu M$), and the binding for AF647-SNA ($c_{SNA} = 0.2 \mu g/mL$) was measured by flow cytometry and normalized to untreated cells ($n = 6$ experimental replicates). (B) Extended glycocalyx reduces SNA dissociation from RBCs. The remodeled cells equilibrated with AF647-SNA were resuspended in pure buffer, and lectin retention was measured by flow cytometry ($n = 6$ experimental replicates). (C) Extended mucin mimetic glycocalyx drives segregation of SNA-receptor adhesion complexes. Fluorescence micrographs show representative confocal images of RBCs remodeled with mucin mimetic GP-M (green, $c_{GP} = 7.5 \mu M$) and stained with AF647-SNA (red, $c_{SNA} = 0.2 \mu g/mL$). Bar graph represents Pearson's correlation coefficient (R^2) analysis of images for SNA binding to RBCs remodeled with polymers of all three lengths ($c_{GP} = 7.5 \mu M$) ($n > 35$ individual cell images per polymer condition). (D) Glycocalyx crowding limits SNA association with cell surface receptors while stabilizing the resulting adhesion complex. Association (green) and retention (red) of AF647-SNA at the surface of RBCs remodeled with GP-M at increasing concentration were measured by flow cytometry and normalized to untreated cells ($n = 12$ experimental replicates). Values represent averages and SDs; P values were determined by ANOVA (A-C) or student test (D); ns>0.05, **<0.01, ***<0.001, ****<0.0001.

glycocalyx brush, as predicted by the current biophysical model for the behavior of membrane-associated mucins (36). The shielding ability of the mucin mimetics was further enhanced at higher concentrations of SNA (*SI Appendix, Fig. S12*), indicating that the lectin also contributes to glycocalyx crowding once bound to its target receptors.

Mucin Mimetics Drive Lectin Clustering by Increasing Glycocalyx Crowding.

The low levels of colocalization between the mucin mimetics and SNA in the RBC glycocalyx suggest increased clustering of the oligomeric lectin, which may stabilize the binding complex through cross-linking of neighboring sialylated glycoconjugates in the plasma membrane. To confirm enhanced lectin clustering by the GPs, we measured Förster resonance energy transfer (FRET) between SNA probes labeled separately with AF594 (donor) or AF647 (acceptor) fluorophores by fluorescence lifetime imaging microscopy (FLIM). A shortening of the donor excited state lifetime (τ) indicates increased FRET efficiency, and thus reduced distance, between the donor and acceptor fluorophores.

First, RBCs were treated with the SNA labeled with AF594 only for 15 min and imaged by FLIM to establish the fluorescence lifetime of the donor ($\tau = 3.15 \pm 0.02$ ns) (Fig. 4A; $c_{SNA} = 0.2 \mu\text{g/mL}$). Incubation of the cells with equimolar amounts of the donor AF594-SNA and acceptor AF647-SNA probes reduced the donor excited state lifetime ($\tau = 2.53 \pm 0.09$ ns), setting the baseline for SNA proximity in the RBC glycocalyx in the absence of the mucin mimetics. Repeating this experiment in the presence of GP-L ($c_{GP} = 7.5 \mu\text{M}$) further reduced the donor excited state lifetime ($\tau = 1.80 \pm 0.07$ ns), revealing closer spacing of the bound lectins. Control experiments with cells treated with the *seco*-cholestenone

anchor only ($c_{chol} = 7.5 \mu\text{M}$) did not reduce lectin spacing ($\tau = 2.65 \pm 0.21$ ns) compared to RBC controls without mucin mimetic treatment, confirming that the GP domains were responsible for driving lectin clustering.

In the absence of ligand-dependent molecular interactions between the GPs and SNA, the observed clustering of the lectin is likely induced by the biophysical properties and membrane diffusion of the mucin mimetics. Enhanced expression of mucins has been shown to increase glycocalyx crowding, which can manifest through changes in membrane shape and the clustering of cell adhesion complexes (26, 36). We used FRET/FLIM to analyze the crowding of mucin mimetics in the RBC glycocalyx in response to SNA binding by measuring changes in their proximity (Fig. 4D–F). GP-L with identical size and glycan composition were synthesized to display donor (AF488) or acceptor (Cy3) fluorophores with overlapping emission and absorption profiles to enable FRET. RBCs were treated either with polymers containing the donor fluorophore only or with an equimolar mixture of polymers presenting both the donor and acceptor dyes (total $c_{GP} = 15 \mu\text{M}$). FLIM imaging of RBCs remodeled with the GP FRET pair showed significantly reduced donor fluorophore lifetime from $\tau = 2.95 \pm 0.10$ ns to $\tau = 2.42 \pm 0.21$ ns after incubation with SNA ($c_{SNA} = 0.2 \mu\text{g/mL}$) for 15 min. The higher FRET efficiency due to shorter distances between the mucin mimetic probes provides experimental support for increased crowding of the glycocalyx environment in response to SNA binding.

Collectively, the FRET/FLIM experiments showed that the lectin clustering and mucin mimetic crowding phenomena are interconnected and occur simultaneously. If the mucin mimetics forced changes in receptor organization prior to lectin binding, we would

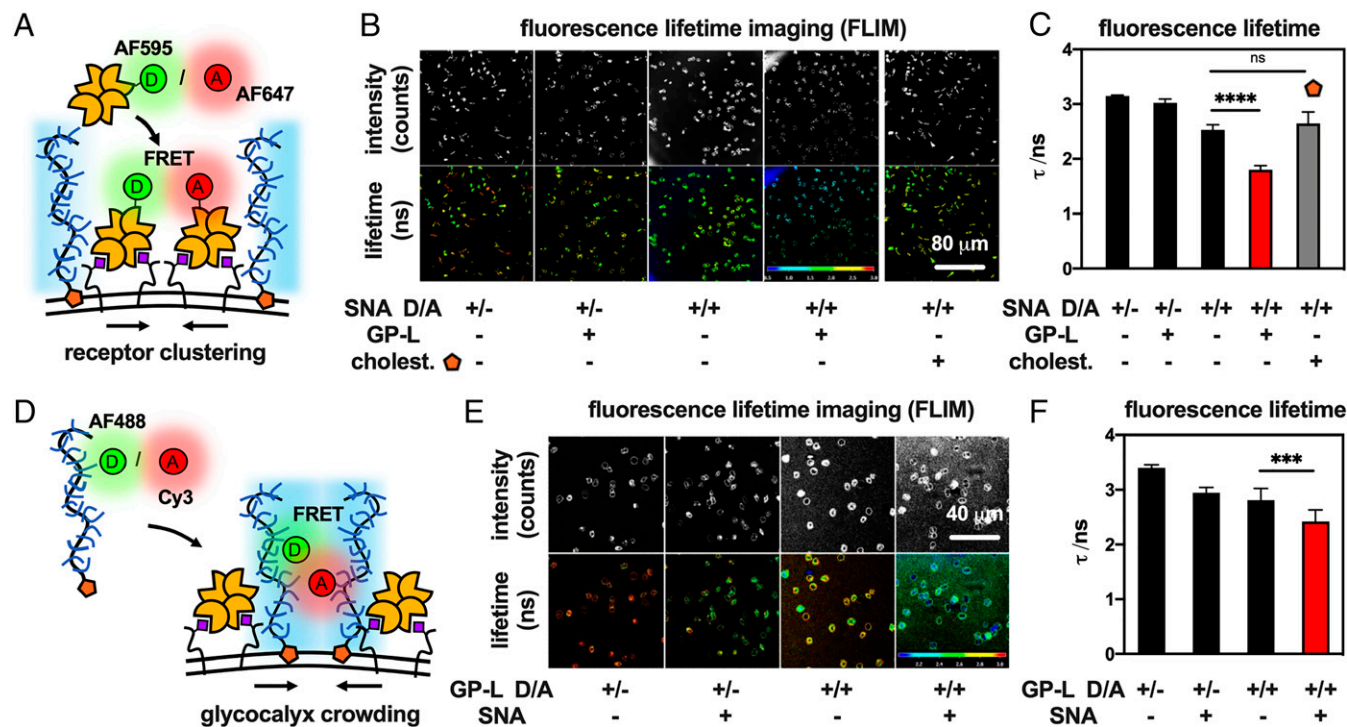


Fig. 4. Glycocalyx crowding drives clustering of lectin-receptor adhesion complexes. (A) Changes in SNA clustering in response to glycocalyx crowding were assessed based on FRET between lectins labeled with donor (D = AF595) and acceptor (A = AF647) probes. (B) Representative FLIM images and (C) bar graph representations for the binding of SNA probes to RBCs before and after remodeling with GP-L ($c_{GP} = 7.5 \mu\text{M}$) or the hydrophobic anchor 5.5 alone ($c_{5.5} = 7.5 \mu\text{M}$). Decrease in fluorescence lifetime (τ) indicates closer SNA proximity. (D) Mucin mimetics labeled with donor (D = AF488) and acceptor (A = Cy3) probes were employed to measure changes in glycocalyx crowding after SNA binding via FRET. (E) Representative FLIM images and (F) bar graph representations of RBCs remodeled with mucin mimetic probes ($c_{GP-D/A} = 15 \mu\text{M}$) before and after incubation with SNA. Decrease in fluorescence lifetime (τ) indicates enhanced glycocalyx crowding. Color scales represent fluorescence lifetime (τ /ns). Values represent averages and SDs for representative image frames containing >10 cells; *P* values were determined by student test; ***<0.001, ****<0.0001.

not expect to observe significant changes in FRET efficiency from the polymers after introduction of SNA. FRAP analysis shows that, once binding equilibrium is reached, the lectins become immobile in the RBC glycocalyx (*SI Appendix, Fig. S13*), providing further support for the stabilization of the SNA binding complexes through clustering and receptor cross-linking.

Glycocalyx Crowding with Mucin Mimetics Enhances H1N1 Virus Retention on RBCs. We sought to evaluate whether the paradox observed for the effect of mucin mimetics on SNA binding, whereby the extended GPs slowed the kinetics of lectin association while stabilizing the resulting binding complex, would also apply to viruses that utilize multivalent receptor interactions for adhesion to host cells. First, we measured the effects of mucin mimetic length and membrane density on the adhesion of the H1N1 virus to RBCs. Cells remodeled with mucin mimetic GPs of all three lengths ($c_{GP} = 7.5 \mu\text{M}$) alongside untreated controls were incubated with H1N1 (33 hemagglutination units [HAU]) for 15 min. The binding experiments were performed at room temperature to limit NA activity and viral release from the cell surface. After incubation, H1N1 binding was detected using an NA enzymatic assay with the fluorogenic reporter substrate, 4-methylumbelliferyl *N*-acetyl- α -neuraminic acid (4-MU-NANA) at 37 °C (38). The rate of fluorescence signal generation by NA activity was used to determine the concentration of RBC-bound viruses in the sample (*SI Appendix, Fig. S14*). All three mucin mimetics reduced the overall amount of virus bound to the RBCs compared to nontreated cells (Fig. 5A). The efficiency of viral binding inhibition correlated with polymer length, increasing from ~20% for the short mimetic GP-S to ~50% for the long polymer GP-L, consistent with enhanced shielding of cell surface receptors by the progressively extended glycocalyx. The shielding capacity of the mucin mimetic glycocalyx against viral adhesion increased with membrane density of the polymers and reached maximal effectiveness at the threshold polymer concentration associated with changes in RBC shape and sedimentation properties (Fig. 5B; $c_{GP-M} = 6.3 \mu\text{M}$). As observed for SNA, increasing viral titers reinforced the protective properties of the mucin mimetics, presumably, by further increasing local crowding in the glycocalyx (*SI Appendix, Fig. S15*).

Analysis of H1N1 retention on RBCs confirmed the ability of the mucin mimetic glycocalyx to stabilize the adhesion complex between the virus and its sialoglycan receptors at the cell surface (Fig. 5C). RBCs remodeled with GPs of all three lengths ($c_{GP} = 7.5 \mu\text{M}$) as well as untreated control cells were first allowed to equilibrate with H1N1 (33 HAU) for 30 min, and then they were washed to remove any unbound virus and resuspended in free buffer for 60 min to allow for dissociation. The experiments were carried out at room temperature to minimize NA activity. The levels of virus bound to the RBC surface before and after dissociation were measured via the 4-MU-NANA fluorescence NA activity assay as described above. Mucin mimetic polymers of all three lengths increased the amount of H1N1 that was retained at the cell surface (75 to 80%) compared to untreated RBC controls (57%). As observed for SNA, the effect of polymer size on enhancing H1N1 retention was less prominent compared to the inhibition of viral binding (Fig. 3B), pointing to a polymer density-driven stabilization of the adhesion complex.

Discussion

Membrane-associated mucins contribute to the protection of epithelial surfaces against pathogen invasion in two distinct ways. Mucins present decoy receptors for capturing pathogens and shedding them from the cell surface. Their organization into a dense extended brush also presents a physical barrier blocking pathogens from accessing functional receptors at the cell surface. Examining how each mechanism contributes to the protection of

host cells against pathogen invasion may guide the development of new therapeutics targeting early stages of infection.

While a range of techniques exist to profile the glycan-binding specificity of pathogen-associated adhesion proteins, the repertoire of tools to study the biophysical properties of the mucin glycocalyx remains limited. Recently, genetic tools have begun to emerge that enable expression of recombinant mucins with precisely defined lengths and membrane densities in cells. This has provided new insights into how the composition and physical properties of the mucin glycocalyx contribute to membrane shape generation (36) and modulation of cell adhesion (39). Although the structure of mucins can now be tailored, tuning their glycosylation state (e.g., the removal or addition of Sias) without affecting other glycoproteins and glycolipids at the cell surface remains a challenge. This makes decoupling the decoy receptor and physical barrier functions of membrane-associated mucins in protecting cells against pathogens difficult, particularly in instances when both protective mechanisms are deployed simultaneously.

One example where membrane mucins serve both purposes is in preventing IAV adhesion to host cells. The mucins are heavily sialylated and capture IAVs by binding to the viral HA proteins. And, while the Sia decoys are rapidly removed by viral NAs, the mucins remain on the cell surface and continue to pose a physical barrier against the virus. Genetic studies identified mucin MUC1 as an important factor in limiting H1N1 infection by shedding the bound virus from the cell surface after the mucin is proteolytically cleaved (17). Virus-induced mucin shedding occurs through proteolytic cleavage in membrane-proximal regions of the protein [e.g., the sea urchin sperm protein, enterokinase, and agrin (SEA) domain (40)] and can trigger downstream signaling to counteract the infection (13). Although the inhibition of IAV binding by physically shielding nonmucin Sia receptors on the cell surface is yet to be demonstrated, studies with *Helicobacter pylori* lacking the mucin adhesins, BabA and SabA, showed inhibition of bacterial infection with increased MUC1 expression (16).

To examine the biophysical principles through which membrane-associated mucins limit pathogen association with host cells, we have generated artificial glycocalyx models of the mucin-like brush on the surfaces of RBCs, which present a biologically relevant environment with respect to receptor complexity and heterogeneity. Using synthetic GPs with tunable size displaying nonparticipating model glycans and endowed with hydrophobic plasma membrane anchors and fluorescent optical probes, we were able to tailor the features of the mucin mimetic brush with respect to size and density and characterize its dynamics. Using our RBC-based mucin glycocalyx model, we systematically evaluated how the length and membrane density of the mucin mimetics influences both binding and dissociation of SNA and H1N1 at the cell surface. By selecting glucose as the side-chain glycan residue for our mimetics, we ensured that the probes would not interact with SNA, H1N1, or any other endogenous glycan-binding protein on the RBC surface. Therefore, any observed changes in lectin or viral binding could be ascribed solely to the biophysical properties of the glycocalyx component.

Installation of the mucin mimetics on the RBC surface introduced significant glycocalyx crowding, which manifested by changes in cell shape toward more rounded morphology, consistent with recent studies showing that increased expression of mucins by cells enforced membrane curvature (36). The change in morphology was accompanied by altered sedimentation properties of the cells, indicating changes in the physical properties of the glycocalyx. FRAP experiments confirmed that the polymers retained their mobility in the glycocalyx through lateral diffusion in the membrane, and the rate of diffusion was inversely correlated to polymer length, indicating physical interactions of the extramembrane GP domain with endogenous glycocalyx components. Analysis of SNA and H1N1 binding near the threshold polymer density associated with morphological and sedimentation changes in the

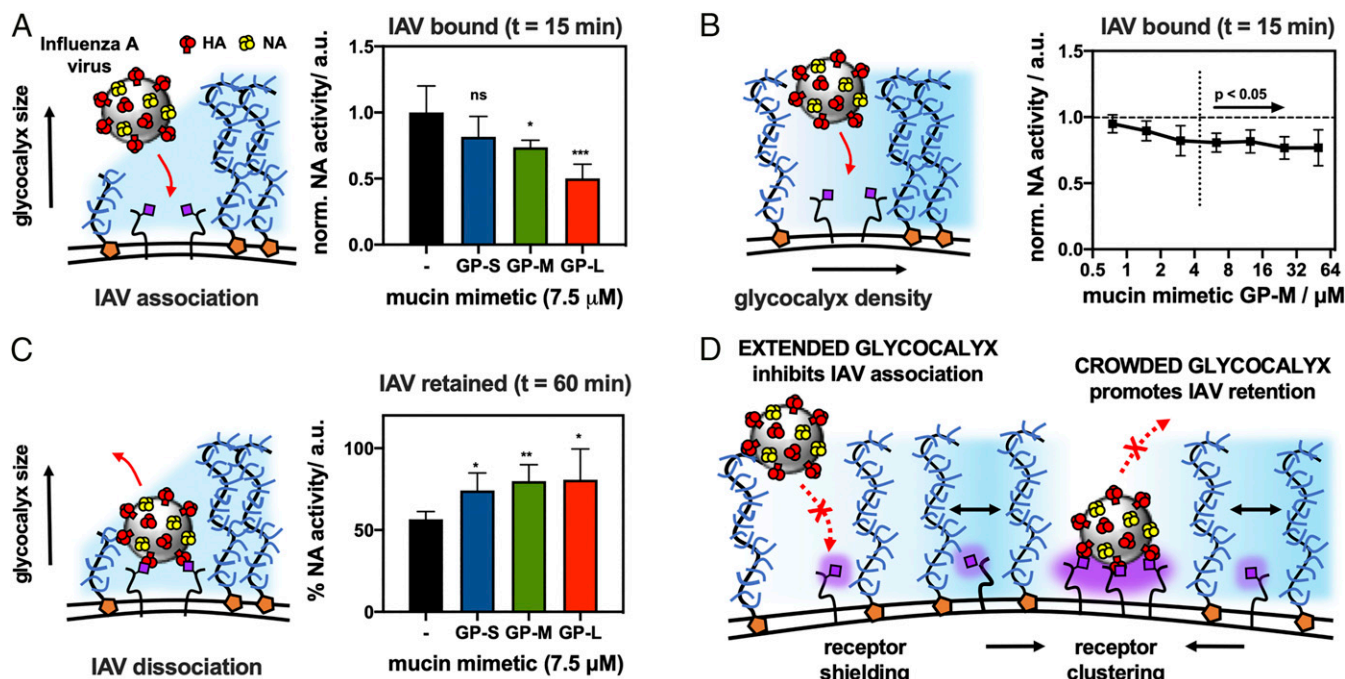


Fig. 5. Influence of glycocalyx size and density on the binding of H1N1 viruses to sialic acid receptors on RBCs. (A) Extended glycocalyx shields endogenous sialic acid receptors from H1N1 binding. Saturation binding of H1N1 ($t = 15$ min) to RBCs remodeled with S, M, and L mucin mimetics GP ($c_{GP} = 7.5 \mu\text{M}$) was assessed via their NA activity toward a fluorogenic substrate 4MU-NANA. (B) Increased glycocalyx crowding limits viral adhesion. Saturation binding of H1N1 ($t = 15$ min) to RBCs remodeled with increasing concentrations of GP-M ($c_{GP} = 0.8 \mu\text{M}$ to $50.0 \mu\text{M}$) was evaluated via NA activity assay with 4MU-NANA. (C) Extended glycocalyx enhances retention of viruses bound to RBC receptors. Retention of H1N1 viruses by RBCs remodeled with mucin mimetics GP of increasing length ($c_{GP} = 7.5 \mu\text{M}$) was measured as a fraction of NA activity before and after equilibration in fresh buffer ($t = 60$ min). (D) Proposed model for the influence of a spectator mucin-type glycocalyx on cell–pathogen interactions. Extended and dense glycocalyx shields cell surface receptors from viral adhesion. Glycocalyx crowding drives receptor clustering and enhances retention of bound viruses. Values represent averages and SDs for $n = 6$ experimental replicates; P values were determined by t test (A and C) and ANOVA (B): * <0.05 , ** <0.01 , *** <0.001 , **** <0.0001 .

RBCs slowed the association rate of the lectin by ~12 to 16% and reduced the overall amount of virus captured at the cell surface by 20 to 50%. The protective effects of the mucin mimetics were polymer length- and membrane density-dependent, in agreement with the proposed mucin brush shielding model and the recent study by Bertozzi and coworkers (28) reporting inhibition of H1N1 binding to gangliosides by mucin mimetic brushes based on lactosylated poly-L-serine polymers anchored in SLBs.

Unexpectedly, the mucin mimetics enhanced the retention of both SNA (8 to 11%) and H1N1 (18 to 23%) at the RBC surface compared to untreated cell controls. This effect was independent of GP size and appeared to be driven primarily by glycocalyx crowding. This suggests that glycan-binding proteins and pathogens may exploit the crowded glycocalyx interface of the epithelial mucosa to strengthen their association with host cells. Confocal fluorescence microscopy of RBC stained with SNA revealed increased exclusion of the mucin mimetics from the lectin adhesion sites based on their length. FLIM/FRET imaging further showed more extensive clustering of SNA in the presence of the mucin mimetics as well as increased crowding in the excluded mucin brush upon lectin binding. The SNA lectin is highly specific for $\alpha 2,6$ -linked Sias (41), while H1N1 recognizes both receptor types with a preference for $\alpha 2,3$ -sialoglycans (42). Despite their different sialoglycan-binding preferences, the responses of SNA and H1N1 to alterations in the glycocalyx composition were similar, pointing to a shared mechanism responsible for these effects and independent of receptor structure.

Based on our observations, we propose a biophysical mechanism for strengthening of interactions between soluble and virus-associated oligomeric lectins and cell surface glycan receptors (Fig. 5D). Therein, the binding of the protein to its receptors

induces exclusion of the mucin mimetics from the point of contact and induces local crowding in the glycocalyx. To alleviate the crowding developing in the mucin mimetic brush (36), smaller glycoconjugates may diffuse back toward the adhesion complex. If these glycoproteins and glycolipids contain Sia modifications, this would generate a higher-valency adhesion patch increasing lectin clustering and overall avidity of the binding event. The limited effect of polymer size on SNA and H1N1 retention supports the proposed mechanism, as the density of mucins at the cell surface, not their length, has been previously identified as the primary driver of entropic pressure on the cell membrane influencing its shape and stability (36). The rounding of RBCs with increasing mucin mimetic density at their membranes provides further evidence for glycocalyx crowding. The proposed mechanism does not require direct binding of the pathogenic adhesins to mucins but assumes multivalency of their interactions with glycan receptors in the glycocalyx. Since most glycan binding proteins utilize multivalency to achieve avidity, we anticipate that this mechanism will be general and exploited by other pathogens that target glycan receptors in mucosal tissues.

Conclusion

In this study, we have applied cell surface engineering with synthetic mimetics of mucin glycoproteins to model the mucosal glycocalyx. By tuning the nanoscale dimension and membrane density of the materials, we assessed the effectiveness of the physical barrier to restrict lectin and virus adhesion to target receptors. The extended and dense cell surface displays of mucin mimetics inhibited the rate of SNA and H1N1 binding, consistent with the current view of mucins acting as a physical shield protecting the cell surface. We discovered that both the soluble and virus-associated oligomeric

lectins exploited the crowded dynamic glycocalyx interface to strengthen their interactions with cell surface receptors. The mucin mimetics were designed to be refractory to the tested glycan-targeting proteins; as such, the observed behavior was driven by the biophysical properties of the glycocalyx and may be a general feature of the mucosal barrier.

Methods

Detailed methods for the synthesis and characterization of GPs; cell surface engineering and characterization via fluorescence microscopy, FRAP and FLIM; and lectin and viral binding assays are provided in *SI Appendix*. *SI Appendix* contains ¹H NMR, infrared spectral data, and size-exclusion chromatography analysis for GPs, extended microscopy, FRAP and FLIM data, and SNA and H1N1 binding controls.

Data Availability. All study data are included in the article and *SI Appendix*.

ACKNOWLEDGMENTS. We thank the University of California San Diego (UCSD) Microscopy Core facility (via p30 Grant N5047101 from the National Institute of Neurological Disorders and Stroke) for assistance with fluorescence microscopy imaging, and the Glycobiology Research and Training Center for access to tissue culture facilities and analytical instrumentation. We acknowledge the use of facilities and instrumentation supported by the NSF through the UCSD Materials Research Science and Engineering Center, DMR-2011924. We thank Dr. Christopher Fisher for help with H1N1 production and Taryn Lucas for her assistance with NA assays. This work was supported by the NIH Director's New Innovator Award 1DP2HD087954-01. K.G. is supported by the Alfred P. Sloan Foundation (FG-2017-9094) and the Research Corporation for Science Advancement via the Cottrell Scholar Award (Grant 24119). P.G. is supported by the G. Harold and Leila Y. Mathers Foundation. This work was previously included as a chapter in the doctoral thesis of D.J.H.

1. C. M. Szymanski, R. L. Schnaar, M. Aebi, "Bacterial and viral infections" in *Essentials of Glycobiology*, A. Varki et al., Eds. (Cold Spring Harbor Laboratory Press, Cold Spring Harbor, NY, ed. 3, 2015), chap. 42, pp. 2015–2017.
2. M. Cohen, A. Varki, The sialome—Far more than the sum of its parts. *OMICS* **14**, 455–464 (2010).
3. A. Varki, R. L. Schnaar, R. Schauer, "Sialic acids and other nonulosonic acids" in *Essentials of Glycobiology*, A. Varki et al., Eds. (Cold Spring Harbor Laboratory Press, Cold Spring Harbor, NY, ed. 3, 2015), chap. 15, pp. 2015–2017.
4. A. Varki, Sialic acids in human health and disease. *Trends Mol. Med.* **14**, 351–360 (2008).
5. Y. Suzuki, Sialobiology of influenza: Molecular mechanism of host range variation of influenza viruses. *Biol. Pharm. Bull.* **28**, 399–408 (2005).
6. B. R. Wasik, K. N. Barnard, C. R. Parrish, Effects of sialic acid modifications on virus binding and infection. *Trends Microbiol.* **24**, 991–1001 (2016).
7. F. Broszeit et al., N-glycolylneuraminic acid as a receptor for influenza A viruses. *Cell Rep.* **27**, 3284–3294.e6 (2019).
8. E. M. Rapoport, L. V. Mochalova, H. J. Gabius, J. Romanova, N. V. Bovin, Search for additional influenza virus to cell interactions. *Glycoconj. J.* **23**, 115–125 (2006).
9. L. Byrd-Leotis et al., Influenza binds phosphorylated glycans from human lung. *Sci. Adv.* **5**, eaav2554 (2019).
10. S. J. Stray, R. D. Cummings, G. M. Air, Influenza virus infection of desialylated cells. *Glycobiology* **10**, 649–658 (2000).
11. R. D. Cummings, R. L. Schnaar, J. D. Esko, K. Drickamer, M. E. Taylor, "Principles of glycan recognition" in *Essentials of Glycobiology*, A. Varki et al., Eds. (Cold Spring Harbor Laboratory Press, Cold Spring Harbor, NY, ed. 3, 2009), chap. 29, pp. 2015–2017.
12. M. Matrosovich, G. Herrler, H. D. Klenk, Sialic acid receptors of viruses. *Top. Curr. Chem.* **367**, 1–28 (2015).
13. A. P. Corfield, Mucins: A biologically relevant glycan barrier in mucosal protection. *Biochim. Biophys. Acta* **1850**, 236–252 (2015).
14. C. E. Wagner, K. M. Wheeler, K. Ribbeck, Mucins and their role in shaping the functions of mucus barriers. *Annu. Rev. Cell Dev. Biol.* **34**, 189–215 (2018).
15. M. A. McGuckin, S. K. Lindén, P. Sutton, T. H. Florin, Mucin dynamics and enteric pathogens. *Nat. Rev. Microbiol.* **9**, 265–278 (2011).
16. S. K. Lindén et al., MUC1 limits *Helicobacter pylori* infection both by steric hindrance and by acting as a releasable decoy. *PLoS Pathog.* **5**, e1000617 (2009).
17. J. L. McAuley et al., The cell surface mucin MUC1 limits the severity of influenza A virus infection. *Mucosal Immunol.* **10**, 1581–1593 (2017).
18. O. Blixt et al., A high-throughput O-glycopeptide discovery platform for seromic profiling. *J. Proteome Res.* **9**, 5250–5261 (2010).
19. M. Kilcoyne et al., Construction of a natural mucin microarray and interrogation for biologically relevant glyco-epitopes. *Anal. Chem.* **84**, 3330–3338 (2012).
20. R. Nason et al., Display of the human mucinome with defined O-glycans by gene engineered cells. *Nat. Commun.* **12**, 4070 (2021).
21. C. Werlang, G. Cárcarmo-Oyarce, K. Ribbeck, Engineering mucus to study and influence the microbiome. *Nat. Rev. Mater.* **4**, 134–145 (2019).
22. D. Rabuka et al., Hierarchical assembly of model cell surfaces: Synthesis of mucin mimetic polymers and their display on supported bilayers. *J. Am. Chem. Soc.* **129**, 5462–5471 (2007).
23. S. C. Purcell, K. Godula, Synthetic glycoscapes: Addressing the structural and functional complexity of the glycocalyx. *Interface Focus* **9**, 20180080 (2019).
24. J. E. Hudak, S. M. Canham, C. R. Bertozzi, Glycocalyx engineering reveals a Siglec-based mechanism for NK cell immunoevasion. *Nat. Chem. Biol.* **10**, 69–75 (2014).
25. D. Rabuka, M. B. Forstner, J. T. Groves, C. R. Bertozzi, Noncovalent cell surface engineering: Incorporation of bioactive synthetic glycopolymers into cellular membranes. *J. Am. Chem. Soc.* **130**, 5947–5953 (2008).
26. M. J. Paszek et al., The cancer glycocalyx mechanically primes integrin-mediated growth and survival. *Nature* **511**, 319–325 (2014).
27. D. J. Honigfort, M. H. Zhang, S. Verespy III, K. Godula, Engineering of spectator glycocalyx structures to evaluate molecular interactions at crowded cellular boundaries. *Faraday Discuss.* **219**, 138–153 (2019).
28. C. S. Delaveris, E. R. Webster, S. M. Banik, S. G. Boxer, C. R. Bertozzi, Membrane-tethered mucin-like polypeptides sterically inhibit binding and slow fusion kinetics of influenza A virus. *Proc. Natl. Acad. Sci. U.S.A.* **117**, 12643–12650 (2020).
29. M. Valeri et al., Pathogenic *E. coli* exploits SslE mucinase activity to translocate through the mucosal barrier and get access to host cells. *PLoS One* **10**, e0117486 (2015).
30. R. Wiggins, S. J. Hicks, P. W. Soothill, M. R. Millar, A. P. Corfield, Mucinases and sialidases: Their role in the pathogenesis of sexually transmitted infections in the female genital tract. *Sex. Transm. Infect.* **77**, 402–408 (2001).
31. M. Cohen et al., Influenza A penetrates host mucus by cleaving sialic acids with neuraminidase. *Virology* **10**, 321 (2013).
32. M. Gervais, A. Labbé, S. Carloti, A. Deffieux, Direct synthesis of α -azido, ω -hydroxypolyethers by monomer-activated anionic polymerization. *Macromolecules* **42**, 2395–2400 (2009).
33. C. W. Tornøe, C. Christensen, M. Meldal, Peptidotriazoles on solid phase: [1,2,3]-triazoles by regioselective copper(i)-catalyzed 1,3-dipolar cycloadditions of terminal alkynes to azides. *J. Org. Chem.* **67**, 3057–3064 (2002).
34. S. Weinbaum, X. Zhang, Y. Han, H. Vink, S. C. Cowin, Mechanotransduction and flow across the endothelial glycocalyx. *Proc. Natl. Acad. Sci. U.S.A.* **100**, 7988–7995 (2003).
35. S. Rad, H. J. Meiselman, B. Neu, Impact of glycocalyx structure on red cell-red cell affinity in polymer suspensions. *Colloids Surf. B Biointerfaces* **123**, 106–113 (2014).
36. C. R. Shurer et al., Physical principles of membrane shape regulation by the glycocalyx. *Cell* **177**, 1757–1770.e21 (2019).
37. A. J. Bradley, K. L. Murad, Regan, M. D. Scott, Biophysical consequences of linker chemistry and polymer size on stealth erythrocytes: Size does matter. *Biochim. Biophys. Acta BBA - Biomembr.* **1561**, 147–158 (2002).
38. M. Cohen et al., Capture and characterization of influenza A virus from primary samples using glycan bead arrays. *Virology* **493**, 128–135 (2016).
39. C. R. Shurer et al., Genetically encoded toolbox for glycocalyx engineering: Tunable control of cell adhesion, survival, and cancer cell behaviors. *ACS Biomater. Sci. Eng.* **4**, 388–399 (2018).
40. D. H. Wreschner et al., Generation of ligand-receptor alliances by "SEA" module-mediated cleavage of membrane-associated mucin proteins. *Protein Sci.* **11**, 698–706 (2002).
41. N. Shibuya et al., The elderberry (*Sambucus nigra* L.) bark lectin recognizes the Neu5Ac(α 2-6)Gal/GalNAc sequence. *J. Biol. Chem.* **262**, 1596–1601 (1987).
42. B. Meng, A. C. Marriott, N. J. Dimmock, The receptor preference of influenza viruses. *Influenza Other Respir. Viruses* **4**, 147–153 (2010).